How to cite: *Angew. Chem. Int. Ed.* **2022,** *61,* e202205251
International Edition: doi.org/10.1002/anie.202205251
German Edition: doi.org/10.1002/ange.202205251

Surface Chemistry | Very Important Paper

Role of Nanoscale Roughness and Polarity in Odd–Even Effect of Self-Assembled Monolayers

*Chuanshen Du, Zhengjia Wang, Jiahao Chen, Andrew Martin, Dhruv Raturi, and Martin Thuo**

Abstract: The dependency of substrate roughness on wetting properties of self-assembled monolayers (SAMs) has been studied extensively, but most previous studies used limited selection of probing liquid and range of surface roughness. These studies disregarded the limit to observation of sub-nanometer odd–even parity effect, hence are inconclusive. In this work we report the role of solvent polarity on the roughness-dependency of wetting behavior of SAMs by studying static con-tact angle of a variety of probing liquids, with different polarities, on SAMs formed on Ag-based substrate with different surface morphology. By overlapping the roughness ranges with previous studies on Au, the limitation of surface roughness (RMS = 1 nm) to observation of the odd–even effect using water as probing liquid was confirmed, but other probing liquid yielded different roughness-dependent behaviors, with more polar solvent showing more roughness-dependent behavior. Based on these observations, we concluded that there exists a phase-transition like behavior in SAMs due to substrate roughness and molecule chain length, but whose determination is dependent on the probing liquid.

[*] C. Du, Z. Wang, J. Chen, A. Martin, D. Raturi, M. Thuo
Department of Materials Science and Engineering, Iowa State University
2220 Hoover Hall, Ames, IA 50011 (USA)
E-mail: mthuo@iastate.edu
J. Chen, M. Thuo
Micro-electronic research center, Iowa State University
133 Applied Sciences Complex, 1925 Scholl Road, Ames, IA 50011 (USA)
M. Thuo
Biopolymer and Biocomposites Research Team, Center for Bio-plastics and Biocomposites, Iowa State University
1041 Food Sciences Building, Ames, IA 50011 (USA)
and
Department of Electrical Engineering, Iowa State University
2215 Coover Hall, Ames, IA 50011 (USA)

Introduction

Properties of self-assembled monolayers (SAMs) have fascinated us since the effect of deposition of a drop of oil on ripples on a pond was observed.[1] As an important type of material, SAMs have shown unique properties with potential applications in diverse fields such as sensing,[2] molecular electronics,[3] functional coating,[4] surface plasmonic modifications,[5] energy conversion,[6] among others. Although inherently nanoscale materials, SAMs benefit from advances in organic synthesis, and therefore embody the elegance of sub-nanometer tunability (bond-by-bond modification) that is the cornerstone of the latter. This tunability, however, introduces compositional variability (entropy) that challenges a coherent delineation of universally defining rules that would form the basis of the field. Defining these governing rules translates to predictability in properties, an essential component for further development of applications based on SAMs.[7] The well-studied n-alkanethiolate SAMs on coinage metals illustrate the need for careful delineation of the governing rules.[7e–f,8]

We,[7b,d,e,8d,f–i,9] and others,[10] have previously explored the role of length of molecule making up the SAM or substrate properties (roughness and identity) on SAM properties. It is well understood that an odd–even parity exists in the property of n-alkanethiolate SAMs, albeit only for smooth surfaces. This odd–even parity in hydrophobicity is, in part, due to an increase in attractive inter-chain van der Waals forces upon addition of a methyl unit and associated parity-dependent presentation of the terminal methyl. Observation of such sub-nanometer structural manifestation had been the basis of the Whitesides–Porter disparity that was latter pinned to substrate roughness.[8d,f] Substrate roughness, therefore, has a significant impact on SAM structure and/or any measurable property (Figure 1a). The odd–even parity effect in hydrophobicity, for example, decays linearly with roughness for SAMs on Au[7d,8g] with an observation limit for surface roughness root mean square, $R_{rms} \approx 1$ nm.[7d,8i] It therefore follows that the odd–even parity effect in hydrophobicity is an appropriate probe for the quality of SAM order, as perturbations by substrate roughness leads to its decay.[7d,8g,i] This decay has been correlated to molecular conformations, molecular length, and dichotomy of the associated energies (polar, E^{p}*, and dispersive, E^{d}*) through χ_c (a parameter others have referred to as the Thuo–Chen constant).[7e,11] But roughness is challenging to quantify given the stochastic distribution of atomically flat regions (grains) on the substrate,[8g] hence the need for a

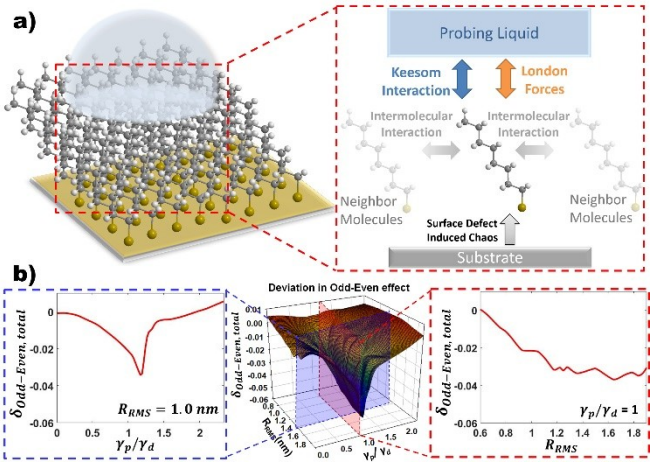

Figure 1. a) A schematic overview of the self-assembled monolayers highlighting attributes that can affect wetting. Wetting on SAMs is a complicated equilibration of the various forces acting on the molecules as indicated. b) Summary of contact angle data using odd–even asymmetry showcasing the phase-transition like behavior driven via both probe liquid and substrate roughness.

rigorous statistical analysis of the data.[12] Even with the smoothest surfaces, given the nanoscale nature of SAMs and associated thermal-driven ($k_B T \neq 0$, T = temperature, k_B = Boltzmann constant) stochasticity, the observed property may depend on probe properties.[13] Wetting properties, for example, depend on the equilibration of forces between the probe liquid and the SAM surface—that is dependent on the substrate hence, wetting depends on both the properties of the probe liquid and the substrate.[8i] Despite challenges associated with understanding the coupled manifestation in substrate roughness, molecular structure, and substrate properties (identity and faceting), comprehensive understanding of SAMs requires convergent studies across these variables. This complexity makes basic measurements, like wetting, multi-dimensional tasks that converge to an equilibrium state based on underlying interactions/forces (Figure 1a).

To quantitively analyze and understand changes in contact angle and solve the discrepancy associated with probe liquids, we adopted the Owens–Wendt–Kaelble (OWK) model for work of adhesion to expand the well-known Young–Dupre's equation,[14] in an effort to separate associated dispersive forces from polar forces, the two major forces affecting wetting [Eq. (1)].[7d,e,14,15]

$$\cos(\theta_s) = 2\left(\frac{\sqrt{\gamma^d_{SG}\gamma^d_{LG}}}{\gamma_{LG}} + \frac{\sqrt{\gamma^p_{SG}}\gamma^p_{LG}}{\gamma_{LG}}\right) - 1 \qquad (1)$$

Since n-alkanethiolate SAMs have a weak dipole moment,[7f] surface interactions are dominated by dispersive forces. From the OWK model, we deduce that the dispersive component of interaction energy, $E^*_d = \sqrt{\gamma^d_{SG}\gamma^d_{LG}}$, while the analogous polar component, $E^*_p = \sqrt{\gamma^p_{SG}\gamma^p_{LG}}$. Based on previous studies,[7d,8b–e,16] we can deduce the effect of certain modification on the SAM. First, as molecular chain length increases, E^*_d decreases as a result of more constrained molecular vibration due to intermolecular interactions.[8c,16] On the other hand, E^*_p would increase both with significant decrease (hyperconjugation in very short hydrocarbons) and increase (enhanced rigidity hence amplification of contribution of surface normal dipole) in molecular chain length.[7d,8b,d,e,17]

Properties of SAMs, however, are not dependent on a singular contributor—e.g., probe liquid polarity, surface roughness, or structure of the molecule, but rather a combination of factors. A dependency of the odd–even oscillation in θ_s on substrate roughness and probe liquid can be captured by normalizing the intra-parity differences to the smoothest surface. Using the average differences in each of the series, we define an average inter-parity static contact angle, $\delta^{Ag^{M-TS,\,X}}_{O-E}$, such that;

$$\delta^{Ag^{M-TS,\,X}}_{O-E} = \left|\cos\bar{\theta}^{Ag^{M-TS,X}}_{odd} - \cos\bar{\theta}^{o}_{odd}\right| - \left|\cos\bar{\theta}^{Ag^{M-TS,X}}_{even} - \cos\bar{\theta}^{o}_{even}\right| \qquad (2)$$

Where, $\cos\bar{\theta}^{Ag^{M-TS,X}}_{odd}$ and $\cos\bar{\theta}^{Ag^{M-TS,X}}_{odd}$ represent the average static contact angle with a probe liquid X formed on a substrate Ag^{M-TS}, while $\cos\bar{\theta}^{o}_{even}$ and $\cos\bar{\theta}^{o}_{odd}$ are the analogous average contact angle on the smooth Ag^{TS}. We capture this interdependency in Figure 1b using evolution in the wetting odd–even effect across different molecular lengths, roughness and with changing probe liquids. The coupled interaction of these factors has not previously been demonstrated in a single plot. Inspired by phase-transition theory, an asymmetry in certain properties could be expected at or near the boundary conditions. At a roughness R_{rms} greater than the previously deduced odd–even limit,[7d,8i,18] an asymmetry in the odd–even effect ($\delta_{odd-even}$) that depends on the properties of the probe liquid (γ_p/γ_d) and roughness is observed. With increasing roughness, a prominently observable asymmetry in the odd–even effect is observed around the polarity equivalence point $\gamma_p = \gamma_d$ (Figure 1b, left), while a pseudo-parabolic evolution is observed with increasing roughness (Figure 1b right). This correlation between surface roughness, probe liquid, and the odd–even asymmetry suggests that perturbation of the order in the SAM by substrate roughness significantly affects the contribution of polar and dispersive interactions at the interface.

Herein we demonstrate the validity of this approach using wetting and population-independent estimation plots to quantitatively evaluate the contribution of each of these system attributes. We then look for convergence points (coherent trends) through Fourier transform of the generated data fits, revealing principle diagonal trends. We demonstrate that properties of self-assembled monolayers are riddled with complexity that calls for careful analysis if we are to realize the full potential of these unique and highly tunable supramolecular nanostructures.

Results and Discussion

The two primary attributes that we aim to evaluate in this work are the coupled role of substrate roughness and probing liquid polarity on wetting properties of SAMs. Based on previous studies, we limit molecular chain lengths to the C_{10}–C_{16} range.[7e,10j,19] Substrates with different surface roughness were used in this work, *viz*; Ag^{TS}, $Ag^{Zn\text{-}TS}$, $Ag^{Ti\text{-}TS}$ and $Ag^{Cu\text{-}TS}$. All four substrates were prepared as previously described and characterized using atomic force microscopy (AFM) to determine their root-mean-square roughness (R_{rms}) and associated bearing volume (BV). For clarity, we based our discussions on R_{rms} given its wide use. The roughness of these substrates are: Ag^{TS} $R_{rms}=0.63\pm0.08$ nm, $BV=0.0059\pm0.0008$ μm^3; $Ag^{Zn\text{-}TS}$ $R_{rms}=1.15\pm0.17$ nm, $BV=0.0094\pm0.0036$ μm^3; $Ag^{Ti\text{-}TS}$ $R_{rms}=1.53\pm0.13$ nm, $BV=0.0203\pm0.0055$ μm^3; $Ag^{Cu\text{-}TS}$ $R_{rms}=1.89\pm0.18$ nm, $BV=0.0209\pm0.0092$ μm^3. The Ag^{TS} roughness falls within the previously determined limit to the odd–even effect (albeit using Au surfaces), while $Ag^{Zn\text{-}TS}$ falls just outside the 1 nm transition limit.[7d,19] The others, $Ag^{Ti\text{-}TS}$ and $Ag^{Cu\text{-}TS}$, extend the roughness range to previously unexplored regions. Four different probe liquids were used in this work, *viz*; hexadecane ($\gamma^p=0$ mN m^{-1}, $\gamma^d=27.5$ mN m^{-1}), ethylene glycol ($\gamma^p=16$ mN m^{-1}, $\gamma^d=32.8$ mN m^{-1}),[20] glycerol ($\gamma^p=30$, $\gamma^d=34$),[21] and water ($\gamma^p=51.0$ mN m^{-1}, $\gamma^d=21.8$ mN m^{-1}).[20] For clarity, we classify the probe liquids based on the ratio of polar and dispersive component of surface tension (γ_p/γ_d) such that the order based on the dominant force is: hexadecane ($\gamma_p/\gamma_d=0$) < ethylene glycol ($\gamma_p/\gamma_d=0.5$) < glycerol ($\gamma_p/\gamma_d=0.9$) < water ($\gamma_p/\gamma_d=2.3$). Besides substrate and probe liquid variables, we explored wetting across different lengths of n-alkanethiol across the so-called waxy region (C_{10}–C_{14}) and into the solid/crystalline region ($\geq C_{14}$). For clarity, and simplicity, we first compare trends in static contact angles (θ_s) across these substrates, probe liquid, and molecule variables prior to quantifying, and ranking, their independent contribution to wetting properties. Given that the equilibrium contact angle is a manifestation of force balance between the SAM surface and the probe liquid, we compared changes in the cosine of the contact angle ($\Delta\cos\theta_s$) with changes in length of the molecule to decouple the parity odd–even effect from substrate and probe liquid effects. We employ population-independent statistics to decouple the magnitude of contribution of each of the variables hence delineate its impact on interfacial properties.

General Trends

As expected,[7c,e,8b,c,f,i] we observed a general increase in θ_s as molecular length increases. The parity odd–even effect, however, decayed with increase in roughness and/or γ_p/γ_d. All probe liquids showed an odd–even effect on the smooth Ag^{TS} ($R_{rms}=0.63$ nm), further confirming the existence of a roughness-dependent limit to this parity effect. Increasing surface roughness ($Ag^{M\text{-}TS}$), however, showed a probe-liquid dependent odd–even effect (Figure 2).

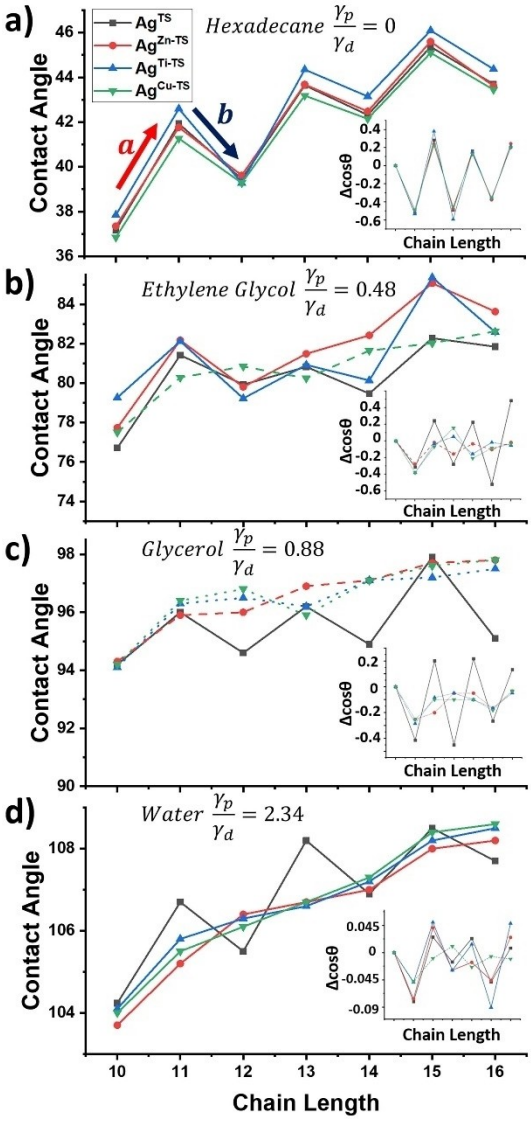

Figure 2. Static contact angles derived from different probe liquids and n-alkanethiol SAMs on substrates bearing different R_{rms}. a) hexadecane, b) ethylene glycol, c) glycerol, d) water. For clarity, the C_{10} normalized change in the cosine of the contact angle was captured in the insertion to further highlight length-dependent trends.

With hexadecane (HD, $\gamma_p/\gamma_d=0$) as probe liquid, SAMs formed on all substrates regardless of roughness showed odd–even effect (Figure 2a). We observe that the odd-parity thiols have higher contact angles than the homologous evens, with the difference between a preceding even- to odd-parity transition being larger than odd to even change, i.e., $(\theta_s^E \rightarrow \theta_s^O) > (\theta_s^O \rightarrow \theta_s^E)$—for brevity, abbreviated "a" and "b" respectively (Figure 2a). The average asymmetry is $\cos\theta \approx 0.6°$ (Insert, Figure 2a). We observe that this difference decreases with increase in molecular length, further supporting the prior inference that a transition point in the structure of the SAM is likely across $C_{13/14}$.[7d,e,8b,h,i] Borrowing from the critical point, T_c, in phase transformation, we infer that the C_{10}–C_{14} range in chain length is analogous to a system transitioning across two phases (e.g. liquid-solid)

hence it is information rich. We, therefore, infer that wetting data across the C_{12}–C_{14} lengths can be used to capture subtle changes in interfacial force equilibration (thermodynamic relaxation), hence inform other properties of SAMs akin to theory in phase transition and criticality (e.g. Landau's theory and the role of order).[22]

With a slight increase in polarity, albeit with dispersive forces still dominating the interactions, i.e., $\gamma_p/\gamma_d \approx 0.5$, (i.e., ethylene Glycol, EG, as probe liquid), a more chaotic trend is observed (Figure 2b). We observe that only Ag^{TS} shows an odd–even effect across the length of the molecules (Figure 2b), albeit unlike in HD, the increase in difference between odd and even parity molecules continue into the crystalline regime ($\geq C_{14}$) for Ag^{TS} but gets chaotic across the $C_{12\text{-}14}$ lengths with increase in roughness (Insert Figure 2b). Increasing the R_{rms} to 1.15 nm ($Ag^{Zn\text{-}TS}$), the parity effect breaks into three with C_{10}–C_{12} and C_{14}–C_{15} showing an oscillation while C_{12}–C_{14} shows a linear increase in θ_s (Figure 2b). Whereas this is clear, and in line with a C_{13} transition, we exercise caution in over-interpretation of the underlying phenomena. This breakdown in the odd–even parity effect increases with increasing roughness. We infer that increasing the polar component of surface tension leads to enhanced distinction of subtle changes in interfacial forces as SAM structure is perturbed by increasing substrate roughness and molecular length. When the contact angles are normalized to the C_{10}, change in $\cos\theta$ clearly shows a parity and roughness dependence (Insert Figure 2b) that rapidly decays across the 1 nm R_{rms} limit. We note that $\Delta\cos\theta$ oscillates between ± 0.2 for C_{10}–C_{14} but is ± 0.5 for C_{14}–C_{16}, the latter being comparable to HD values while the former shows significantly diminished parity effect on Ag^{TS}. A parity-dependent oscillation, albeit significantly reduced, is observed at $R_{rms} = 1.15$ nm.

When the dispersive and polar forces are almost equal, $\gamma_p/\gamma_d \approx 0.9$, (Glycerol), we see further decay in the odd–even effect with increase in surface R_{rms} (Figure 2c). All surfaces, except Ag^{TS}, did not show any odd–even parity effect but rather a gradual increase in θ_s is observed (Figure 2c). Normalizing $\Delta\cos\theta$ to C_{10}, the lack of parity effect is clearly observed as all values, except for Ag^{TS}, show no zigzag oscillation. These results further support the inference that gradually tuning γ_p in the probe liquid reveals quality of the SAM. Interestingly, parity oscillation can be deduced from the edges of the length scale investigated here, further supporting our inference that the $C_{12\text{–}14}$ window likely captures criticality of the equilibrating forces.

Finally, when polar interactions dominate interfacial interactions $\gamma_p/\gamma_d \approx 2.3$, (water), no odd–even parity is clearly observable for all surfaces except Ag^{TS} (Figure 2d). A gradual increase in θ_s is observed in all surfaces with $R_{rms} >$ 1 nm continuing the trend in loss of the odd–even parity effect with increase in γ_p. From the C_{10} normalized $\Delta\cos\theta$, however, we observed very weak oscillation ($\approx \pm 0.05$) whose margin is not amenable to interpretation (insert Figure 2d). Despite the low values, the general trends in these oscillations are larger for the edges C_{10}–C_{12} and C_{14}–C_{16} but are significantly diminished in the mid region (C_{12}–C_{14}). This is the exact opposite of what is observed with HD (insert Figure 1a), but becomes predominant with increase in γ_p. This observation, albeit subtle, is likely correlated with a property of the SAM, which we infer to be order (symmetry) akin to phase change.

A closer look at the trends in the C_{10} normalized $\Delta\cos\theta$ shows a complicated trend across each length scale. For example, for $Ag^{Cu\text{-}TS}$ (green line), the parity oscillation in C_{10}–C_{13} is larger and inverse to that observed for C_{14}–C_{16} (insert Figure 2d).

Given the complexity (multi-dimensional nature) of the obtained data, it is important that we further investigate this data set using population-independent statistics (estimation plots and unpaired mean differences) to quantify role of substrate, molecular length, and probe liquid properties in wetting and, by extension, the SAM structure.

Effect of Substrate Roughness on Hydrophobicity of SAMs

We apply estimation plots and associated unpaired mean differences in contact angles ($\Delta\bar{\theta}$) to deduce the effect of probe liquid or roughness on the contact angles. For brevity, we discuss data derived from SAMs on the edge of the waxy (C_{10}) and the crystalline (C_{14}) regions— we provide other data in the Supporting Information (Figure S1, S2). The smoothest surface, Ag^{TS} was used as the reference point given the previously established odd–even limit of $R_{rms} =$ 1 nm. As shown in Figure 3, we observed an asymmetric trend in wetting with polar and non-polar solvents with changes in substrate roughness. We note that for HD $\Delta\bar{\theta} \leq 0$ with increase in R_{rms}—except for C_{14} SAM on $Ag^{Ti\text{-}TS}$. Negative $\Delta\bar{\theta}$ implies that increase in roughness favors wetting (lower θ_s) with HD. Specifically, for HD on C_{10} (waxy region) on $Ag^{Zn\text{-}TS}$ (Figure 3a), $\Delta\bar{\theta} = -4°$, while $Ag^{Ti\text{-}TS}$ and $Ag^{Cu\text{-}TS}$ decreased θ by 0° and 1.8°, respectively. For HD on C_{14} SAM, however, a decrease ($Ag^{Zn\text{-}TS}$ and $Ag^{Cu\text{-}TS}$ $\Delta\bar{\theta} \approx -2°$) and increase ($Ag^{Ti\text{-}TS}$ $\Delta\bar{\theta} = 1.9°$) was observed (Figure 3b).

Intermediate polarity liquids ethylene glycol, EG, ($\gamma_p/\gamma_d = 0.49$) and glycerol (($\gamma_p/\gamma_d = 0.88$) showed comparable asymmetric trends in $\Delta\bar{\theta}$ with increasing R_{rms}. The $\Delta\bar{\theta}$ for EG and glycerol does not significantly change with roughness except for EG on $Ag^{Ti\text{-}TS}$ ($R_{rms} = 1.53 \pm 0.13$ nm) SAMs. We observe that $\Delta\bar{\theta} \geq 0$ indicating that roughness leads to increased de-wetting for these medium polarity probe liquids. For EG on C_{10}, $\Delta\bar{\theta} = 1°$, 3°, and 0.9° for $Ag^{Zn\text{-}TS}$, $Ag^{Ti\text{-}TS}$, and $Ag^{Cu\text{-}TS}$ respectively (Figure 3c)' while on C_{14} SAM, EG gave $\Delta\bar{\theta} = 3°$, 0.9°, and 2.0° for $Ag^{Zn\text{-}TS}$, $Ag^{Ti\text{-}TS}$, and $Ag^{Cu\text{-}TS}$ respectively (Figure 3d). For glycerol on C_{10} SAM, $Ag^{Zn\text{-}TS}$ gave $\Delta\bar{\theta} = 0.4°$ compared to $\Delta\bar{\theta} = -0.2°$ and 0 on $Ag^{Ti\text{-}TS}$ and $Ag^{Cu\text{-}TS}$ respectively (Figure 3e). Similarly, for glycerol on C_{14} SAMs, all three substrates gave $\Delta\bar{\theta} = 2.8°$ (Figure 3f).

When the probe liquid is changed to water (Figure 3g and h) increase in roughness gave $\Delta\bar{\theta} \leq 0$ indicating enhanced wettability. We observe an analogous general trend (increase then decrease) in $\Delta\bar{\theta}$ for the shorter (C_{10}) SAM, but a gradual decay for the solid-like (C_{14}) SAMs. For water on C_{10}, a decrease in $\Delta\bar{\theta} \approx -1.2°$, $-0.7°$, and $-1.6°$ were observed with increase in R_{rms} from 0.63 nm to 1.15 nm

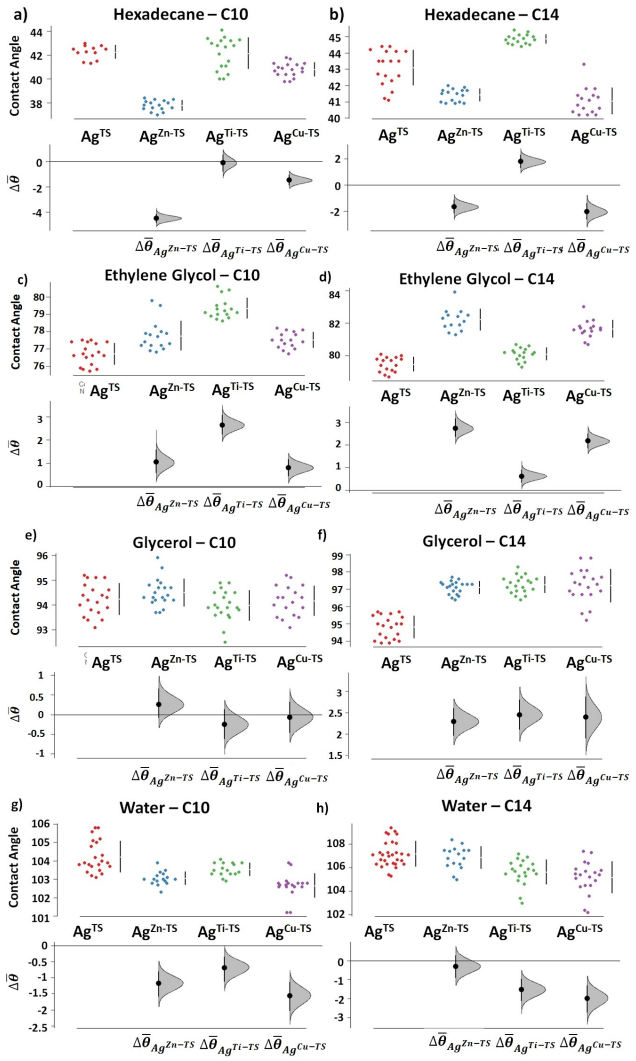

Figure 3. Roughness-dependent wetting behavior of SAMs probed with liquids of different polarity.

($Ag^{Zn\text{-}TS}$), 1.5 nm ($Ag^{Ti\text{-}TS}$), and 1.9 nm ($Ag^{Cu\text{-}TS}$) respectively (Figure 3g). When this is evaluated on the solid-like SAM (C_{14}), a gradual decrease in $\Delta\bar{\theta} \approx -0.3°$, $-1.5°$, $-1.9°$ is observed over the same substrate roughness range (Figure 3h). We note that the latter shows a linear decay in $\Delta\bar{\theta}$, indicating that an increase in roughness leads to increase in wettability with water for these rather hydrophobic molecules. We infer that this increased wettability suggesting the likely decrease in dominance of the surface properties by the molecule. The effect of roughness, therefore, does not align with the general trend in θs, implying that a more dominant factor, other than substrate roughness, might be at play in the overall wetting behavior. We infer that substrate roughness, in this context, may abet droplet pinning akin to the rose petal effect.[23] For brevity and clarity, we have so far limited the comparative analysis to even numbered SAMs even though we are aware of the odd–even parity effect. To fully comprehend the interdependency of roughness, molecular chain length and wetting properties, an integration of these three variables into a surface profile is needed.

Effect of Molecular Chain Length on Asymmetry in Odd–Even Effect

To understand the contribution of molecular chain length in wetting, pairwise comparison of consecutive homologs can reveal the role of an odd vs even orientation and how this evolves with substrate roughness and/or polarity of the probe liquid. Using estimation plots, we calculate the unpaired mean difference ($\Delta\bar{\theta}$) with addition of a single carbon, first for a) $\theta_s^E \rightarrow \theta_s^O$ (Figure 4a–d) then b) $\theta_s^O \rightarrow \theta_s^E$ (Figure 4e–h) in the non-wetting (water) data. For smooth surfaces, $R_{rms} = 0.63$ nm (Ag^{TS}, Figure 4a), the $C_{10\text{-}11}$ transition yielded a 2.6° increase in θ, a large change than for $C_{12\text{-}13}$ (0.9°) and $C_{14\text{-}15}$ (1.0°). Increasing substrate roughness to

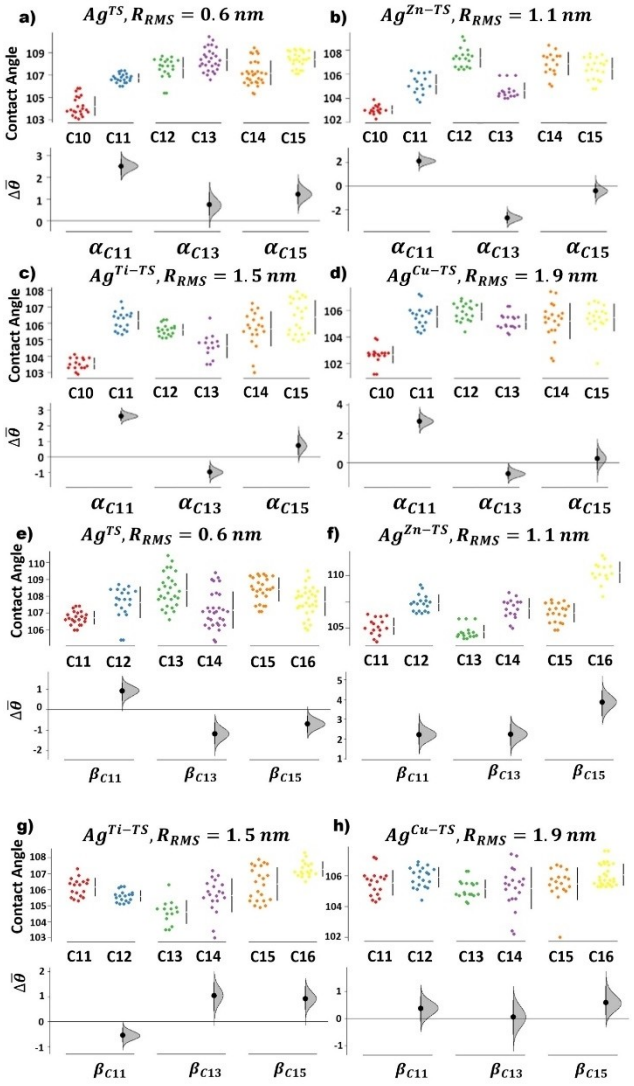

Figure 4. Summary of pairwise comparison of the effect of altering the length of the alkanethiol by a CH_2. We separate the transitions into "a" ($\theta_s^E \rightarrow \theta_s^O$) and "b" ($\theta_s^O \rightarrow \theta_s^E$) as previously described in Figure 2a.

$R_{rms}=1.15$ nm ($Ag^{Zn\text{-}TS}$, Figure 4b) the $C_{10\text{-}11}$ transition yielded a 2.0° increase in θ, while $C_{12\text{-}13}$ and $C_{14\text{-}15}$ transition caused a decrease in θ, of −2.2° and −0.2° respectively. Further increase in roughness $R_{rms}=1.5$ nm ($Ag^{Ti\text{-}TS}$, Figure 4c) and $R_{rms}=1.9$ nm ($Ag^{Cu\text{-}TS}$, Figure 4d), showed an increase in θ for $C_{10\text{-}11}$ transition (2.5° and 3.1° respectively), but a decreasing θ for $C_{12\text{-}13}$ transition (−1° and −0.6°) and a minimal change in θ for $C_{14\text{-}15}$ transition (0.9° and 0.3°). From these data we can infer that the C_{10}-$_{11}$ pair behaves consistently i.e., favors dewetting, while trends in higher molecular lengths depends on the substrate roughness with chain length playing minimal role for rougher surfaces.

On the other hand, *b* angles ($\theta_s^O \rightarrow \theta_s^E$) yields slightly different trends. For the smooth Ag^{TS} (Figure 4e), the $C_{11\text{-}12}$ transition leads to a 1° increase in θ, while the $C_{13\text{-}14}$ and $C_{15\text{-}16}$ transition decreased θ by 1.1° and 0.8° respectively. On $Ag^{Zn\text{-}TS}$, all transition led to increased θ by 2.1°($C_{11\text{-}12}$), 2.1° ($C_{13\text{-}14}$) and 3.9° ($C_{15\text{-}16}$). On $Ag^{Ti\text{-}TS}$, however, $C_{11\text{-}12}$ transition led to a 0.4° decrease in θ, while the $C_{13\text{-}14}$ and $C_{15\text{-}16}$ raised θ 1.0° (Figure 4f and g). On $Ag^{Cu\text{-}TS}$ (Figure 4h) Change in length had minimal effect on contact angle with $C_{11\text{-}12}$, $C_{13\text{-}14}$, and $C_{15\text{-}16}$ transition showing statistically insignificant changes in θ values with $\Delta\bar{\theta}\approx 0°$(0.3°, 0.1° and 0.5° respectively). As observed above, the trend in contribution of molecular chain length to role of surface roughness-dependent wettability is asymmetric across $R_{rms}\approx 1$ nm as captured here with enhanced wetting (decreasing $\Delta\bar{\theta}$) for $R_{rms}<1$ nm and dewetting (increasing $\Delta\bar{\theta}$) for $R_{rms}>1$ nm.

We infer that, generally, increase in molecular length enhances de-wetting, hence de-pinning of the droplet, akin to increased texturing in creation of self-cleaning surfaces and the lotus leaf effect (vis-à-vis the rose petal effect).

Comparison of Roughness and Solvent-Dependent Behaviors between Odd and Even SAMs

For quantitative analysis of θ_s, we recognized that substrate roughness and probe liquid characteristics are independent variables. Molecular chain length and terminal methyl group orientation, however, are coupled by the structure of SAMs.[7e] We observed that odd- and even-SAMs have different sensitivities to different perturbations (Figure 4), hence are different homologous series. This present a quandary in that, one cannot discuss a continuum in length while negating the subsequent asymmetry in properties, unless chain length is discussed as a parity-dictated dichotomous characteristic. Periodic oscillation in the orientation of the terminal moiety (Figure 1a) dictates that any discussion of SAM properties be pinned on this dichotomous structural homology rather than the commonly used continuum based on length (Å or nm) or number of carbons.

To further understand parity effects in SAMs, we analyzed integrated changes in the cosine of the contact angles after adding one carbon onto an odd SAM ($\Delta\cos\theta_{odd}$, from average of "b") or an even-SAM ($\Delta\cos\theta_{even}$, from average of "a") with both changes in probe (γ_p/γ_d), and roughness (R_{rms}). To linearize the properties of the probe liquid, for direct comparison with the R_{rms}, we use the logarithm [$\ln(\gamma_p/\gamma_d)$]. Fitting the data to a surface gives a heat map that captures the coupled effect of surface roughness and probe liquid properties (Figure 5). From $\Delta\cos\theta_{odd}$ (Figure 5a) and $\Delta\cos\theta_{even}$ (Figure 5b), a diagonal trend is observed with a blue to red (bottom left to top right) and blue to green (bottom right to top left) diagonals emerging. From Figure 1b, however, a transition is observed at $\gamma_p=\gamma_d$ albeit as perturbed by the previously observed[8d,17] small surface normal dipole on the SAM. This coincides with the previoustransitions in phase of the SAMs, hence emboldens us to infer that these heatmaps do capture the surface properties of the SAM irrespective of their structural or electronic origin(s). Considering the x-axis, a transition seems to appear around the $R_{rms}=1.5$ nm, albeit this broadens with increase in γ_p/γ_d to cover the 1–1.5 nm range (purple region, Figure 5a and b). Based on these two transitions, a hypothetical demarcation of the plot at $\ln(\gamma_p/\gamma_d)\approx 0.8$ and $R_{rms}=1.5$ nm leads to a quadrant (Figure 5d). Assuming a drive towards convergence, a Fourier transformation of the plot reveals minor convergent points (figure 5c) that line up along the diagonals with emergence of a "central valley". The applicability of a Fourier transform reveals convergence —navigating towards an equilibrium,[24] of the underlying behavior along the principal diagonal where a row of peaks emerge. Orthogonal symmetry in peak heights in the off-axis is also observed (Figure 5c). These heatmaps, therefore, present a qualitative view of the interfacial interactions as dictated by the three variables, *viz*; probe liquid, substrate roughness, and molecular length, hence we can deduce that each of the resulting quadrants represents domination of the surface by one of these variables.

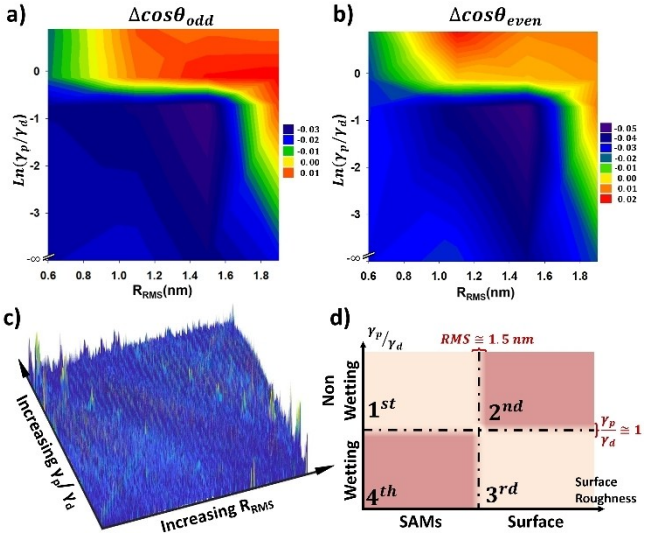

Figure 5. Integrated roughness and probe liquid dependent behavior of SAMs. a) The effect of probe liquid and roughness on even-to-odd SAMs contact angle changes. b) The effect of probe liquid and roughness on odd-to-even SAMs contact angle changes. c) Illustrative Fourier transformation of (a) revealing the convergence points while forming a central diagonal valley. d) A schematic summary of the wetting behavior and the probe-liquid vs. surface roughness capture in a so-called "scarlet quadrant".

From correlations above, we infer that there is an interdependency of properties of a SAM on substrate properties (roughness) and, for wetting, dispersive/polar forces, with certain regions dominated by either factor. We divide this into a quadrant with each of the four quadrants illustrating a domination by one or combination of the two effects -for brevity we refer to this as the "scarlet quadrant". It is therefore critical that properties of SAMs be described using a similar quadrant (or analogous presentation) to abet delineation, and avoid misinterpretation, of observed data. Adopting the scarlet quadrant (Figure 5d), the first half on the *x*-axis captures the SAM-dominated properties, while the second half is the dominated substrate characteristics. Similarly, on the *y*-axis, the bottom is dominated by non-polar interactions while the top is dominated by polar interactions. We infer that the first corner (bottom left, 4th quadrant, blue color) captures a region dominated by the SAM and symmetric (non-polar) interactions, while the top left (1st quadrant, green color) captures the SAM dominated asymmetric interactions. Analogously, the 2nd and 3rd quadrants capture polar and non-polar interactions albeit dominated by substrate roughness. The presence of a "valley" on the top-left to bottom-right diagonal, however, indicates a likely divergence on the coupled behavior. To illustrate this delayed divergence in the dataset, a 3D rendering of the data is essential.

Big Picture: Understanding the Effect of Substrate Roughness and Probe Liquid on Asymmetric Odd–Even Oscillation in θ_s

Given the observed dependency of the odd–even oscillation in θ_s on substrate roughness and probe liquid, as captured by $\delta_{O-E}^{Ag^{M-TS,\,X}}$, we further simplify this relation such that;

$$\delta_{O-E}^{Ag^{M-TS,\,X}} = \left|\cos\bar{\theta}_{odd}^{Ag^{M-TS,X}} - \cos\bar{\theta}_{odd}^{o}\right| - \left|\cos\bar{\theta}_{even}^{Ag^{M-TS,X}} - \cos\bar{\theta}_{even}^{o}\right| \quad (3)$$

Can be shortened to;

$$\delta_{O-E}^{Ag^{M-TS,\,X}} = \Delta\cos\theta_{odd} - \Delta\cos\theta_{even} \quad (4)$$

For each of the homologous parity series, we plot the normalized difference in θ_s ($\Delta\cos\theta_{odd}$ or $\Delta\cos\theta_{even}$) We observe analogous trends in $\Delta\cos\theta$ across the homologous parity (SAM^E vs. SAM^O) series (Figure 5a vs. b), with changes in substrate R_{rms} and probe liquid properties, affirming that this is a viable inter-parity comparison parameter. We note that probe liquid properties are plotted on a logarithm scale while R_{rms} is linear. We analyze this data to inform the coupled dependency.

i) *Effect of substrate roughness on the probe liquid Wetting:* Figure 5a shows that the change in contact angle due to change in probe liquid is mostly similar for SAM^E and SAM^O. When substrate roughness is low, difference in surface normal dipole would keep the hydrophobicity of SAM^E and SAM^O slightly apart, leading to a clear odd–even effect. As substrate roughness increases, SAMs formed on such substrates can no longer pack well, and the small surface normal dipole is perturbed, hence SAMs effectively becoming a layer of chaotic hydrocarbons, that is a layer of "fat" as previously noted by Whitesides and co-workers.[25] With increasing substrate roughness, however, we observed a solvent dependency on the asymmetry in wetting of SAMs, highlighted by the difference in slope of the boundary around top-left corner of figure 5a and b. This difference is also summarized in the deep valley shown on the left-center panel of Figure 1b.

ii) *Impact of probe liquid on deducing the effect of substrate roughness on the asymmetric wetting in SAMs.* On the other hand, we noticed similar yet different trend studying the effect of substrate roughness with different probe liquid. Analogous to observation above, solvent with a high γ_p/γ_d and solvent with a low γ_p/γ_d both give analogous wetting behaviors (Figure 3a vs. b). Solvent with moderate γ_p/γ_d, however, can reveal regions where substrate roughness changes can lead to different response between SAM^E and SAM^O (Figure 4). Although asymmetry in wetting behavior may necessitate tuning substrate roughness and probe liquid (Figure 5c), their tolerance to each of this variable is different. From the shape of the valley in the center of figure 5c, as well as the shape of the two center panels, we notice that there exists a wider tolerance for substrate roughness than for γ_p/γ_d (probe liquid) in realizing the asymmetry in SAM wetting.

iii) *Surface properties of SAMs are complicated and need careful, deliberate description*: Extending the arguments above to the 3D rendering of this rather complex property, we observe that the normalize cosθ is initially linear (flat) for smooth surfaces ($R_{rms} \leq 1$ nm). Between $R_{rms} = 1$–1.5 nm, and $\gamma_p/\gamma_d = 0.8$, a rapid decline in the normalized $\cos\bar{\theta}_{odd}^{Ag^{M-TS,X}}$ is observed creating a valley from which the polar and non-polar interactions diverge. This figure captures the roughness-dependent wetting properties and highlights the need to discuss roughness of a surface in any study of SAMs if coherence is to be obtained across different measurements.

Conclusion

From the statistical analysis of contact angle data of SAMs with different probing liquids and substrate roughness, we may infer that:

Controlling Substrate Roughness Is Critical to Revealing Sub-Nanometer Properties of SAMs

As demonstrated, properties of SAMs depend on several factors that interfere, to varied extents (as captured by the estimation plots) with each other. In order to maximize effect of molecular properties it is necessary to maintain a

substrate that would induce least defects in the formed SAMs. This is especially important if unfavorable interaction (non-wetting) occur on the top (unbound) interface of SAMs.

A Progressive Limit to the Odd–Even Parity Effect in Hydrophobicity of n-Alkanethiolate SAMs Was Observed

The previously deduced limit to the odd–even effect in wetting with water was confirmed.[7d] We also mapped the progression of this limit with change in the polar component of surface tension of the probe liquid. This progressive limit, while derived from Ag-based SAMs, could also be applicable to Au-based n-alkanethiolate SAMs upon adjustments for associated differences, similar to differences in odd–even effects for n-alkanethiolate SAMs on Au and Ag substrates.[13]

There Exists an Interdependency of Substrate Roughness, Molecular Length, Probe Liquid Polarity and Surface Properties of SAMs

We confirmed that changing the probing liquid can significantly change the limit to odd–even effect, a phenomenon indicating well packed-SAMs.[7d,e,8h] We were also able to create a heatmap summarizing the state of the SAMs based on the developed asymmetry parameter (Figure 1b), which can be further divided into four quadrants as shown in Figure 5d:

Quadrant 1: Molecule/Polar interaction dominated. With a non-wetting solvent as probe liquid and smooth surface, we can observe clear, symmetric odd–even effect. Compared with quadrant 4, wetting system that fall in this region highlights possible polar interaction between the hydrophobic SAMs and the probe liquid.

Quadrant 2: Surface/Polar interaction dominated. With non-wetting solvent as probe liquid and rough surface, intermolecular interactions within SAMs are greatly suppressed and little to no structure–property relationship tied to the molecule would be revealed. Wetting within this quadrant is likely chaotic (due to disorder), hence properties represent an ensemble average of all possible SAM-liquid configuration and therefore wetting is asymmetry.

Quadrant 3: Surface/Dispersive interaction dominated. With a wetting solvent as probe liquid and rough surface, we can still observe odd–even effect, though the amplitude may be reduced and the oscillation is no longer symmetric. Dispersive interaction dominated wetting scenario abets the intermolecular interactions within SAMs to overcome minor surface defects caused by surface roughness, helping to retain certain structure–property relationship.

Quadrant 4: Molecule/Dispersive interaction dominated. With a wetting solvent as probe liquid and smooth surface, we can observe clear, symmetric odd–even effect. In this quadrant, the smooth substrate induces minimal number of defects within SAMs, leading to predictable structure-wetting relationship. This is the quadrant that dominate most of the work on SAMs since any contact is considered to be an insignificant perturbation.

This work resolves the Whitesides–Porter discrepancy by illustrating the complex nature of wetting behavior while giving pre-eminence to the need to clearly report substrate properties. The inferences draw here also inform fields that deploy SAMs by illustrating the need to consider any, and all, interface perturbations on the SAMs to inform potential shifts in the equilibrium structure. By understanding role of polar and non-polar interactions at the interface, one can predict potential interferences by either the substrate or object/liquid contacting the SAM as depicted in the scarlet quadrant. The assumption that all measurements are limited to quadrant 4 is a simplification of otherwise complex processes.

Experimental Section

Materials: All alkanethiols were purchased from Sigma–Aldrich except n-Tridecyl mercaptan (C13) which was purchased from Pfaltz&Bauer. 200 proof ethanol was purchased from Decon Laboratories, Inc. All chemicals and reagents were used as received. Nitrogen and argon gas (UHP) were purchased from Airgas and used as supplied.

Preparation of silver substrate: Metal films were custom prepared by Substrata Thin Film Solutions Inc or prepared by e-beam evaporation as previously described.[7c,d,8f,h,10h,i] For example, a 200 nm Ag film was first evaporated onto an atomically flat silicon wafer, then a 10 nm layer of an metal adlayer (Fe, Zn, Cu and Ti) was sputtered onto the Ag film. The metal substrates were template stripped to reveal the ultra-flat surface as previously reported.[7c,d,8d,10a] Glass supports were cleaned using ethanol and blow-dried with UHP nitrogen gas. A piece of the cleaned glass supports was glued on the metal surface with $\approx$8 μL of optical adhesive (Norland Optical Adhesive 61). All bubbles in the glue were gently removed by tapping on the glass. The glue was then cured under a long-wave UV light for 12 hrs.

AFM surface characterization: A Bruker Innova AFM was used in contact mode to characterize the surface features of template-stripped surfaces. Images obtained ranged from 3 to 5 μm in length and width using the highest resolution available (1 Hz). All samples were measured immediately after template-stripping, and surface morphology/roughness analyzed automatically using the NanoscopeAnalysis 2.0 software.

Preparation of monolayers: Freshly template-stripped $Ag^{M\text{-}TS}$ (M = adlayer) pieces were cleaned using ethanol and blow-dried with nitrogen stream. As previously reported, the $Ag^{M\text{-}TS}$ piece were placed in a vial containing 5 mL ethanolic (200 proof) solution of 3 mMol alkanethiol. The surface and thiol solution were incubated for 3hr. The so-formed SAM was cleaned with ethanol and blow-dried with nitrogen gas. All measurements were carried out immediately and lasted for less than 2 hrs.

Measuring the contact angle: Static contact angles formed between the SAMs and probe liquids (deionized (DI) water, hexadecane (HD), ethylene glycol (EG) and glycerol were measured using a Ramé–Hart Goniometer (Model 100-00) with a tilting base. A droplet of the probe liquid (5 μL) was dispensed onto the SAMs through an integrated syringe pump. Images of the droplets sitting on the SAMs were analyzed with the DropImage® software.

Acknowledgements

This work was supported in part by a U.S. Air Force Office of Scientific Research under award number FA2386-16-1-4113 and a Catron fellowship to J.C. Open access funding provided by the Iowa State University Library.

Conflict of Interest

The authors declare no conflict of interest.

Data Availability Statement

The data that support the findings of this study are available from the corresponding author upon reasonable request.

Keywords: Odd–even Effect · Self-Assembly · Surface Engineering

[1] B. Franklin, W. Brownrigg, *Philos. Trans. R. Soc. London* **1774**, 445–460.

[2] a) X. Xu, A. Makaraviciute, S. Kumar, C. Wen, M. Sjödin, E. Abdurakhmanov, U. H. Danielson, L. Nyholm, Z. Zhang, *Anal. Chem.* **2019**, *91*, 14697–14704; b) N. A. S. Omar, Y. W. Fen, J. Abdullah, Y. M. Kamil, W. M. E. M. M. Daniyal, A. R. Sadrolhosseini, M. A. Mahdi, *Sci. Rep.* **2020**, *10*, 2374; c) A. Kaur, S. Kaur, M. Sharma, I. Kaur, *J. Electroanal. Chem.* **2019**, *833*, 221–230.

[3] a) X. Qiu, V. Ivasyshyn, L. Qiu, M. Enache, J. Dong, S. Rousseva, G. Portale, M. Stöhr, J. C. Hummelen, R. C. Chiechi, *Nat. Mater.* **2020**, *19*, 330–337; b) G. D. Kong, S. E. Byeon, S. Park, H. Song, S. Y. Kim, H. J. Yoon, *Adv. Electron. Mater.* **2020**, *6*, 1901157.

[4] a) T. Zhu, J. Su, F. Labat, I. Ciofini, T. Pauporté, *ACS Appl. Mater. Interfaces* **2020**, *12*, 744–752; b) D. Bobb-Semple, K. L. Nardi, N. Draeger, D. M. Hausmann, S. F. Bent, *Chem. Mater.* **2019**, *31*, 1635–1645; c) A. H. Jenkins, C. B. Musgrave, J. W. Medlin, *ACS Appl. Mater. Interfaces* **2019**, *11*, 41289–41296; d) S. Lamping, C. Buten, B. J. Ravoo, *Acc. Chem. Res.* **2019**, *52*, 1336–1346.

[5] a) S. B. Ulapane, N. J. Kamathewatta, H. M. Ashberry, C. L. Berrie, *ACS Appl. Nano Mater.* **2019**, *2*, 7114–7125; b) H. Qian, Y. Huang, X. Duan, X. Wei, Y. Fan, D. Gan, S. Yue, W. Cheng, T. Chen, *Biosens. Bioelectron.* **2019**, *140*, 111350.

[6] a) S.-H. Shin, Y. E. Bae, H. K. Moon, J. Kim, S.-H. Choi, Y. Kim, H. J. Yoon, M. H. Lee, J. Nah, *ACS Nano* **2017**, *11*, 6131–6138; b) S. Park, S. Kang, H. J. Yoon, *ACS Cent. Sci.* **2019**, *5*, 1975–1982; c) L. Cui, R. Miao, K. Wang, D. Thompson, L. A. Zotti, J. C. Cuevas, E. Meyhofer, P. Reddy, *Nat. Nanotechnol.* **2018**, *13*, 122–127.

[7] a) F. Ben Amara, E. R. Dionne, S. Kassir, C. Pellerin, A. Badia, *J. Am. Chem. Soc.* **2020**, *142*, 13051–13061; b) J. Chen, M. Kim, S. Gathiaka, S. J. Cho, S. Kundu, H. J. Yoon, M. M. Thuo, *J. Phys. Chem. Lett.* **2018**, *9*, 5078–5085; c) M. M. Thuo, W. F. Reus, C. A. Nijhuis, J. R. Barber, C. Kim, M. D. Schulz, G. M. Whitesides, *J. Am. Chem. Soc.* **2011**, *133*, 2962–2975; d) J. Chen, Z. Wang, S. Oyola-Reynoso, S. M. Gathiaka, M. Thuo, *Langmuir* **2015**, *31*, 7047–7054; e) J. Chen, B. Chang, S. Oyola-Reynoso, Z. Wang, M. Thuo, *ACS Omega* **2017**, *2*, 2072–2084; f) J. C. Love, L. A. Estroff, J. K. Kriebel, R. G. Nuzzo, G. M. Whitesides, *Chem. Rev.* **2005**, *105*, 1103–1170.

[8] a) D. Prashar, *Int. J. ChemTech Res.* **2012**, *4*, 258–265; b) L. Ramin, A. Jabbarzadeh, *Langmuir* **2011**, *27*, 9748–9759; c) N. Nishi, D. Hobara, M. Yamamoto, T. Kakiuchi, *J. Chem. Phys.* **2003**, *118*, 1904–1911; d) L. B. Newcomb, I. D. Tevis, M. B. Atkinson, S. M. Gathiaka, R. E. Luna, M. Thuo, *Langmuir* **2014**, *30*, 11985–11992; e) A. Nurbawono, S. Liu, C. A. Nijhuis, C. Zhang, *J. Phys. Chem. C* **2015**, *119*, 5657–5662; f) Z. Wang, J. Chen, S. Oyola-Reynoso, M. Thuo, *Coating* **2015**, *5*, 1034–1055; g) Z. Wang, J. Chen, S. M. Gathiaka, S. Oyola-Reynoso, M. Thuo, *Langmuir* **2016**, *32*, 10358–10367; h) J. Chen, Z. Wang, S. Oyola-Reynoso, M. M. Thuo, *Langmuir* **2017**, *33*, 13451–13467; i) Z. Wang, J. Chen, S. Oyola-Reynoso, M. Thuo, *Langmuir* **2016**, *32*, 8230–8237; j) N. D. Aagaard, J. C. Azcárate, J. Olmos-Asar, M. M. Mariscal, J. Solla-Gullón, E. Zelaya, M. H. Fonticelli, *J. Phys. Chem. C* **2020**, *124*, 22591–22600; k) G. Kumar, T. Van Cleve, J. Park, A. Van Duin, J. W. Medlin, M. J. Janik, *Langmuir* **2018**, *34*, 6346–6357.

[9] C. Du, S. R. Norris, A. Thakur, J. Chen, B. VanVeller, M. Thuo, *J. Am. Chem. Soc.* **2021**, *143*, 13878–13886.

[10] a) E. A. Weiss, G. K. Kaufman, J. K. Kriebel, Z. Li, R. Schalek, G. M. Whitesides, *Langmuir* **2007**, *23*, 9686–9694; b) E. A. Weiss, J. K. Kriebel, M.-A. Rampi, G. M. Whitesides, *Phys. Eng. Sci.* **2007**, *365*, 1509–1537; c) R. C. Chiechi, E. A. Weiss, M. D. Dickey, G. M. Whitesides, *Angew. Chem. Int. Ed.* **2008**, *47*, 142–144; *Angew. Chem.* **2008**, *120*, 148–150; d) P. Rothemund, C. Morris Bowers, Z. Suo, G. M. Whitesides, *Chem. Mater.* **2018**, *30*, 129–137; e) C. M. Bowers, K.-C. Liao, T. Zaba, D. Rappoport, M. Baghbanzadeh, B. Breiten, A. Krzykawska, P. Cyganik, G. M. Whitesides, *ACS Nano* **2015**, *9*, 1471–1477; f) F. Mirjani, J. M. Thijssen, G. M. Whitesides, M. A. Ratner, *ACS Nano* **2014**, *8*, 12428–12436; g) M. Baghbanzadeh, F. C. Simeone, C. M. Bowers, K.-C. Liao, M. Thuo, M. Baghbanzadeh, M. S. Miller, T. B. Carmichael, G. M. Whitesides, *J. Am. Chem. Soc.* **2014**, *136*, 16919–16925; h) W. F. Reus, M. M. Thuo, N. D. Shapiro, C. A. Nijhuis, G. M. Whitesides, *ACS Nano* **2012**, *6*, 4806–4822; i) J. R. Barber, H. J. Yoon, C. M. Bowers, M. M. Thuo, B. Breiten, D. M. Gooding, G. M. Whitesides, *Chem. Mater.* **2014**, *26*, 3938–3947; j) L. Jiang, C. S. Sangeeth, L. Yuan, D. Thompson, C. A. Nijhuis, *Nano Lett.* **2015**, *15*, 6643–6649.

[11] S. H. Yu, S. Z. Hassan, G.-H. Nam, S. An, B. Kang, D. S. Chung, *Chem. Mater.* **2021**, *33*, 5991–6002.

[12] J. Sporrer, J. Chen, Z. Wang, M. M. Thuo, *J. Phys. Chem. Lett.* **2015**, *6*, 4952–4958.

[13] a) J. Chen, J. Liu, I. D. Tevis, R. S. Andino, C. M. Miller, L. D. Ziegler, X. Chen, M. M. Thuo, *Phys. Chem. Chem. Phys.* **2017**, *19*, 6989–6995; b) C. Du, R. S. Andino, M. C. Rotondaro, S. W. Devlin, S. Erramilli, L. D. Ziegler, M. M. Thuo, *J. Phys. Chem. C* **2022**, *126*, 7294–7306.

[14] a) D. K. Owens, R. Wendt, *J. Appl. Polym. Sci.* **1969**, *13*, 1741–1747; b) M. E. Schrader, *Langmuir* **1995**, *11*, 3585–3589.

[15] B. Jańczuk, T. Białopiotrowicz, W. Wójcik, *J. Colloid Interface Sci.* **1989**, *127*, 59–66.

[16] T. Iimori, T. Iwahashi, K. Kanai, K. Seki, J. Sung, D. Kim, H.-o. Hamaguchi, Y. Ouchi, *J. Phys. Chem. B* **2007**, *111*, 4860–4866.

[17] L. A. Vogt, Electronic structure predictions for properties of organic materials, Harvard University, **2012**.

[18] Z. Wang, J. Chen, S. Oyola-Reynoso, M. Thuo, *Coating* **2015**, *5*, 1034–1055.

[19] J. Chen, T. J. Giroux, Y. Nguyen, A. A. Kadoma, B. S. Chang, B. VanVeller, M. M. Thuo, *Phys. Chem. Chem. Phys.* **2018**, *20*, 4864–4878.

[20] A. Toussaint, P. Luner, *Contact Angle, Wettability and Adhesion* (Ed.: K. L. Mittal), VSP, Utrecht, **1993**, p. 385.

[21] L. C. Holysz, E. Tenside, *Surfactants Deterg.* **1988**, *25*, 337–339.

[22] a) L. Landau, *Phys. Z. Sowjetunion* **1937**, *11*, 545; b) E. Ising, *Beitrag zur theorie des ferro- und paramagnetismus*, PhD thesis, Grefe & Tiedemann, **1924**; c) K. G. Wilson, *Rev. Mod. Phys.* **1983**, *55*, 583; d) M. E. Fisher, *Rev. Mod. Phys.* **1998**, *70*, 653.
[23] a) J. J. Chang, C. Du, A. Pauls, M. Thuo, *Angew. Chem. Int. Ed.* **2021**, *60*, 13929–13936; *Angew. Chem.* **2021**, *133*, 14048–14055; b) J. J. Chang, A. Martin, C. Du, A. M. Pauls, M. Thuo, *Angew. Chem. Int. Ed.* **2020**, *59*, 16346–16351; *Angew. Chem.* **2020**, *132*, 16488–16493.
[24] a) V. Serov, *Fourier series, Fourier transform and their applications to mathematical physics, Vol. 197*, Springer, Cham, **2017**; b) R. N. Bracewell, R. N. Bracewell, *The Fourier transform and its applications, Vol. 31999*, McGraw-Hill, New York, **1986**.
[25] H. J. Yoon, N. D. Shapiro, K. M. Park, M. M. Thuo, S. Soh, G. M. Whitesides, *Angew. Chem. Int. Ed.* **2012**, *51*, 4658–4661; *Angew. Chem.* **2012**, *124*, 4736–4739.

Manuscript received: April 10, 2022
Accepted manuscript online: May 17, 2022
Version of record online: June 1, 2022